

# Trajectory Optimization for Dynamic Needle Insertion\*

Matt Heverly and Pierre Dupont

Department of Aerospace and Mechanical Engineering  
Boston University  
110 Cummington Street, Boston, MA 02215, USA  
[{mheverly|pierre}@bu.edu](mailto:{mheverly|pierre}@bu.edu)

John Triedman, MD

Department of Cardiology  
Children's Hospital Boston  
300 Longwood Ave., Boston, MA 02115, USA  
[john.triedman@cardio.chboston.org](mailto:john.triedman@cardio.chboston.org)

**Abstract** – Needle based intervention procedures are a common minimally invasive surgical technique. In many of these procedures, the needle can be considered rigid and the tissue deforms and displaces substantially as the needle is advanced to its target. An energy based, fracture mechanics approach is presented to show that the velocity dependence of tissue properties can reduce tissue motion with increased needle velocities. In-vitro test results on porcine heart samples show that the force required to initiate cutting reduces with increasing needle velocity up to a critical speed, above which, the rate independent cutting force of the underlying tissue becomes the limiting factor. In-vivo tests show increased needle speed results in reduced force and displacement for needle insertion into the heart. Results indicate that automated insertion could substantially improve performance in some applications.

**Index Terms** – *Needle Puncture, Needle Cutting, Tissue Dynamics, Surgical Robotics*

## I. INTRODUCTION

In medical interventions, needles are commonly used to reach a target site. These percutaneous procedures are minimally invasive and allow access to tissue structures that would otherwise be difficult or impossible to reach. Examples include biopsies, placement of radioactive seeds at tumor sites and epidural injections in the spinal column. An important developing area is prenatal interventions in which surgical repairs are made to a fetus in utero so that its subsequent development can proceed normally.

A specific example is fetal hypoplastic left heart syndrome in which the left ventricle of the fetal heart fails to develop due to a restriction in the aortic valve. As depicted in Fig. 1, correcting this defect involves inserting a needle into the left ventricle and passing a balloon through the needle into the aortic valve. The balloon is then inflated, which expands the valve, reducing the pressure in the ventricle and allowing it to develop normally.

In most needle-based procedures, insertion is performed slowly with the interventionalist manually guiding the needle to the tissue target. Visualization of both the needle and the target is usually provided using non-invasive methods such as real-time ultrasound. Due to substantial tissue deformation and displacement during needle insertion, constant path corrections must be made in order for the needle to reach its target. Target motion also requires constant adjustment of the ultrasound field of view to track both the needle and the target.

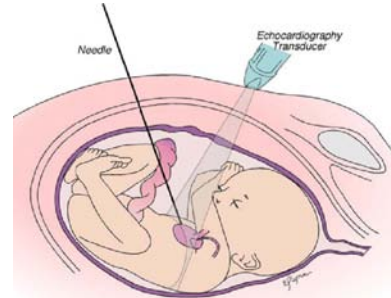


Fig. 1 Overview of percutaneous image-guided fetal cardiac intervention.

In the case of fetal cardiac interventions, postoperative ultrasound video analysis indicates a ventricular insertion velocity of 10-15 mm/sec. Prior to ventricular puncture, the ventricle collapses upon itself and the heart displaces due to motion of the fetus in the uterus as well as compression of tissue supporting the heart in the fetal chest cavity. For ventricular insertion, the needle target can be considered the center point of the chamber. Owing to its collapse under needle loading and sudden expansion after penetration, however, care must be taken not to puncture its posterior wall.

Interventionalists have recognized for some time that faster needle motions result in less tissue deformation and displacement. When working near delicate tissue structures, however, limitations of human motor control and skill level have led to the adoption of the current quasistatic insertion approach. This paper investigates the mechanics associated with needle velocity and the potential for automating insertion motions in the context of ventricular penetration.

## C. Prior Work

Characterization of needle forces in percutaneous surgical procedures has been an active area of research in recent years [1,2], often to create surgical simulators for training purposes [3,4,5,12,13]. Needle cutting data can also be used to automate portions of the needle insertion procedure. For example, Brett *et al.* [6] used characteristics of the force profile to identify tissue boundaries for automated epidural puncture. Effects of friction and tip geometry have been studied [7,8], and Okamura *et al.* [9] have developed a model to separate needle stiffness, friction, and cutting forces. DiMaio and Salcudean considered the interaction of a compliant needle with tissue [10], as well as needle steering [11]. With the exception of [13], the literature treats needle insertion as a quasistatic process.

\* This research was funded by the NIH under Grant #R01 EB003052-01.

While tissue cutting is perhaps the oldest application of tools, the literature devoted to it is extremely limited [14]. The difficulty arises from the complexity of tissue models in comparison to materials such as metals. Mahvash and Hayward do present a fracture mechanics approach to cutting in [15].

The framework of fracture mechanics is adopted in this paper as well to characterize stable and unstable cutting. This approach is presented below. An energy argument incorporating tissue dynamics is made in section 3 to provide a basis for needle trajectory optimization. In-vitro as well as in-vivo experimental results are presented in section 4, illustrating the minimization of displacement and deformation for heart puncture. Conclusions appear in the final section.

## II. MODELING NEEDLE INSERTION

In classical fracture mechanics, the incremental work applied by a cutting tool,  $F dx$ , can be divided as

$$F dx = d\Lambda + d\Gamma + J dA \quad (1)$$

in which  $\Lambda$  is the potential energy and  $\Gamma$  is dissipated energy, which in metals is primarily due to plastic flow [16]. The fracture toughness,  $J$ , is the energy necessary to increase the area of fracture by an incremental amount  $dA$ .

While the structure of tissue is clearly very different from materials for which fracture is well understood, the same general principles can be applied to gain an understanding of tissue cutting [15]. Since cutting dynamics are to be considered, (1) is modified to include a kinetic energy term,  $dH$ , and needle force and displacement are denoted by  $F_n$  and  $dx_n$ , respectively:

$$F_n dx_n = d\Lambda + dH + d\Gamma + J_c ds \quad (2)$$

For needle cutting, this equation also replaces fracture area  $dA$  with incremental cutting depth  $ds$ , yielding a cutting fracture toughness  $J_c$  with units of force.

The relationship between needle displacement  $dx_n$  and cutting depth,  $ds$  is shown in Fig. 2. Since the tissue can displace and deform during cutting, a tissue body frame is defined at each instant which is coincident with the tip of the needle. This frame moves with the uncut tissue by an incremental displacement,  $dx_t$ . In this way, incremental cut depth can be seen to relate to incremental needle displacement as

$$ds = dx_n - dx_t \quad (3)$$

Since  $ds \geq 0$ , this equation implies that the tissue remains in contact with the needle. This is an assumption on the tissue properties that the flow of energy between  $\Lambda$ ,  $H$  and  $\Gamma$  is such that, for the needle trajectories considered, the tissue can always decelerate faster than the needle.

Equation (2) applies both during the initial loading phase before cutting commences as well as during cutting. During the loading phase, no cutting occurs,  $J_c ds = 0$ . Once a critical needle force,  $F_c$ , is reached, cutting

commences either stably or unstably. Idealized force-displacement curves for stable and unstable cutting are depicted in Fig. 3.

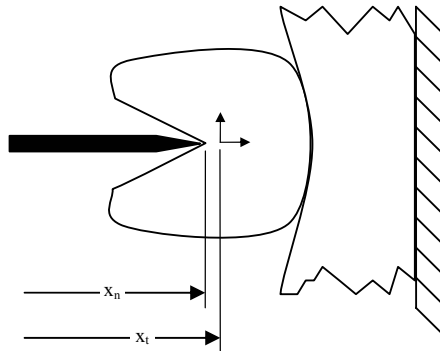


Fig. 2 Cutting diagram.

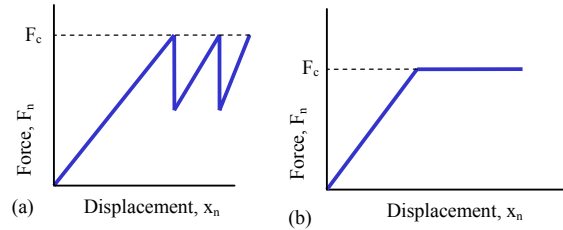


Fig. 3 Force profiles for (a) unstable cutting, (b) stable cutting.

Unstable cutting, shown in Fig. 3(a), is a process in which work done by a cutting tool is first stored as elastic energy and then released quickly when the critical cutting force,  $F_c$  is achieved. While many definitions of stable cutting are possible, (3) suggests that minimum requirements of stability for  $dx_n > 0$  are

$$0 < ds \leq dx_n \quad (4)$$

The lower bound indicates that once cutting begins, cutting depth continues to increase. The upper bound prevents tissue relaxation to the extent that it forces tissue displacement to satisfy  $dx_t \geq 0$ . The important implication of this bound is that cut depth can be controlled by needle displacement so that needle penetration beyond the target site can be avoided.

In fracture mechanics, the phenomenon of unstable cutting is tied to a negative dependence of fracture toughness on crack tip velocity [16]. This is analogous to the phenomenon of stick-slip friction in which a negative dependence of steady-state friction force on slip velocity can lead to unsteady motion.

An idealization of a negatively-sloped cutting force curve is depicted in Fig. 4. As with its frictional counterpart, one way to stabilize cutting is to change the operating point to one of non-negative slope. For the curve in Fig. 4, this corresponds to a cutting velocity of  $\dot{s} \geq \dot{s}_{cr}$ . The idealized stable cutting in Fig. 3(b) would equate to achieving  $\dot{s} \geq \dot{s}_{cr}$  as well.

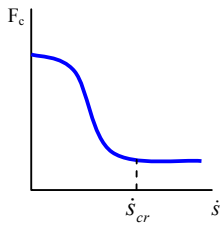


Fig. 4 Steady-state cutting force versus cutting velocity.

### III. TRAJECTORY OPTIMIZATION

The goal of needle insertion is to drive the needle tip to its target with minimum motion of both the target and surrounding tissues. Note, however, that it is the reaction forces associated with the non-cutting work terms in (2) that balance the needle force, so their energy cannot be made zero. Some tissue motion is therefore inevitable, but it is the relative flow of energy into these terms that will be shown to be important to the optimization.

An idealized needle force vs. displacement curve is shown in Fig. 5 illustrating the two phases of needle insertion. Trajectory optimization will be considered separately for the loading, Phase I, and cutting, Phase II, of needle insertion. In the loading phase, the needle force builds to the critical force required to initiate cutting,  $F_c$  which occurs at a displacement  $x_c$ . The second phase begins once cutting is initiated and extends until the tip reaches its target. Since needle forces are small, it is reasonable to take needle velocity as the system input during both phases of cutting.

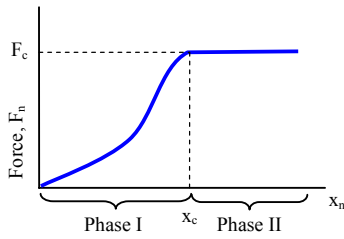


Fig. 5 Needle force vs. displacement during insertion.

#### A. Phase I

In the loading phase, no work is expended in cutting and (2) reduces to

$$\begin{aligned} F_n dx_n &= d\Lambda + dH + d\Gamma \\ dx_n &= dx_t, \quad ds = 0 \end{aligned} \quad (5)$$

This non-cutting work,  $W_{nc}$ , can be rewritten in terms of the reaction forces associated with changes in each of the energy terms as

$$W_{nc} = (F_\Lambda + F_H + F_\Gamma) dx_n. \quad (6)$$

Minimizing tissue motion during this phase is equivalent to minimizing needle displacement,  $x_n = x_c$ , at which the needle force equals the cutting force,  $F_n = F_c$ . Assuming

that if the tissue is loaded quasi-statically,  $F_\Lambda$  is the only significant reaction force, and that it is a monotonically increasing function of  $x_n$ , the displacement  $x_c$  can potentially be reduced by two different dynamic effects. First, if the forces  $F_H$  and  $F_\Gamma$  in (6) can be made positive, any given cutting force will be attained with a smaller  $x_c$  as illustrated in Fig. 6. Secondly, a negative dependence of cutting force on cutting velocity would reduce  $F_c$  and consequently  $x_c$ .

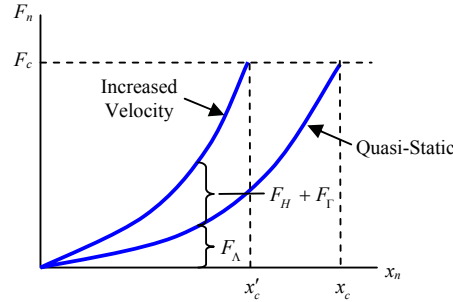


Fig. 6 Needle force vs. needle displacement for quasi-static and high velocity loading curves during phase I

While potential energy is rate independent, the reaction force of kinetic energy is proportional to the rate of change of velocity. In the needle contact zone, tissue is accelerated from rest to the needle velocity, generating a positive reaction force that will increase with needle velocity. Furthermore, tissue dissipative forces, such as arising from fluid flow out of the tissue, are positively dependent on loading rate. The result is that increasing needle velocity can generate larger reaction forces for smaller pre-cutting displacements of the needle.

If the tissue exhibits a negatively-sloped cutting force curve, as illustrated in Fig. 4, increasing needle velocity can also be used to reduce the force required to initiate cutting. Since needle force increases monotonically with needle displacement, this reduced force will decrease the displacement necessary to reach Phase II. If there is a critical cutting velocity  $\dot{s}_{cr}$  above which the cutting force is constant, then any  $\dot{x}_n \geq \dot{s}_{cr}$  will minimize this peak force.

During the loading phase, maximizing the needle velocity minimizes the tissue motion by (i) changing the shape of the loading curve such that the cutting force,  $F_c$ , is reached with a lower displacement and (ii) minimizing the peak force due to the negatively sloped cutting force curve.

#### B. Phase II

The second phase of needle insertion commences with the onset of cutting and concludes when the needle tip reaches its target. To minimize motion of both the target and surrounding tissues, as well as to avoid needle over-penetration, stable cutting is desired. Stable cutting can be achieved by selecting a cutting velocity of non-negative slope on the steady-state cutting force versus velocity curve. If such a point does not exist, it may be possible to modify the slope of the curve by using a sharper cutting tool [16].

Assuming stable cutting, the needle force is given by  $F_n = F_c$  and (2) and (4) can be written as rate equations

$$F_c(\dot{x}_n - \dot{s}) = F_c \dot{x}_t = d\Delta/dt + dH/dt + d\Gamma/dt \quad (7)$$

$$0 < \dot{s} \leq \dot{x}_n$$

The non-cutting power is proportional to  $\dot{x}_t$ , the velocity of the tissue at the cutting interface. It represents the deformation and displacement of the tissue that continues during cutting in reaction to the needle-applied cutting force.

Minimization of tissue motion will be considered for the special case depicted in Fig. 4. For stable cutting,  $\dot{s} \geq \dot{s}_{cr}$  and the cutting force  $F_c$  is constant. The causality of tissue motion is such that  $(x_t(t), \dot{x}_t(t))$ ,  $\forall t$  depend only on the applied force,  $F_c$ .

$$\ddot{x}_t = f(x_t, \dot{x}_t, F_c) \quad (8)$$

The rate version of (3) is

$$\dot{s} = \dot{x}_n - \dot{x}_t \quad (9)$$

which indicates that stability is achieved for  $\dot{x}_n \geq \dot{x}_t + \dot{s}_{cr}$  and, furthermore, by (8), that cutting velocity  $\dot{s}$  increases with needle velocity.

From (8), the change in tissue displacement  $x_t$  can be reduced by reducing the time of application of the cutting force,  $F_c$ . This is accomplished by increasing needle velocity and, by doing so, increasing cutting velocity.

In summary, reducing tissue motion during both the loading and cutting phases of needle insertion involves increasing needle velocity. The following experiments apply this approach to needle cutting of porcine and rabbit cardiac tissue.

#### IV. EXPERIMENTAL RESULTS

Needle insertion tests were performed on in-vitro porcine heart samples as well as in-vivo using rabbits. As shown in Fig. 7, a linear actuator was instrumented with a load cell and a 1.1 mm diameter tri-pointed surgical needle. Force, position, and velocity data were collected at a 2 kHz sample rate as the needle was inserted into tissue samples at various velocities. In all tests, the needle was initially preloaded to a specified force value against the exterior wall of the left ventricle. This preload ensures consistent initial conditions as well as ensuring that the contact area between the needle and tissue is fully developed. Trapezoidal needle velocity profiles with various peak speeds were applied in random order over the surface of a tissue sample.

##### A. Porcine Heart Samples

A series of insertion tests were performed on porcine heart specimens. The hearts were all excised and stored in phosphate buffered saline solution prior to testing to preserve the tissue and testing was started less than 2 hours postmortem. Fig. 8 shows typical force vs. displacement curves for both a low speed and high speed insertion. In this

test, the ventricle wall was removed from the heart and placed on a rigid surface. This has the effect of stiffening the tissue sample since the compliance of the in vivo boundary conditions are replaced by those of the rigid surface. The zero position on the displacement scale represents contact between the needle tip and the rigid support ensuring that the needle had cut through the entire thickness of the tissue.

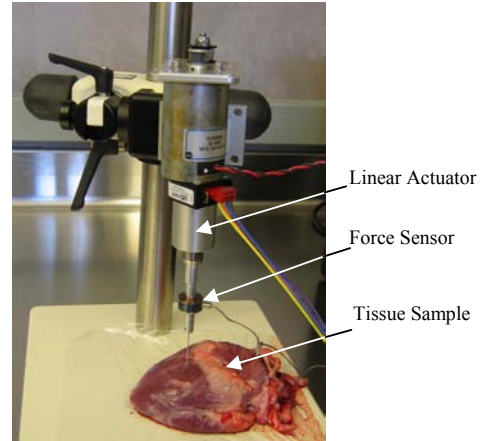


Fig. 7 Needle insertion test setup shown with porcine heart sample.

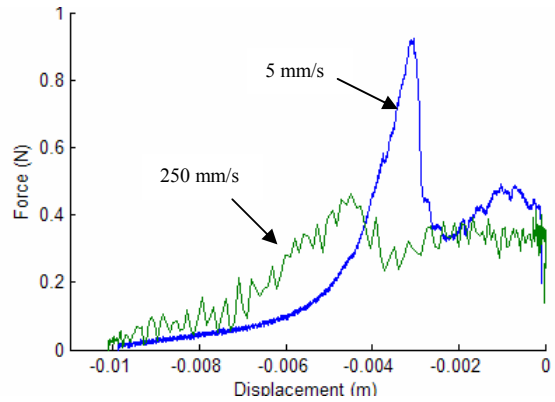


Fig. 8 Needle force vs. needle displacement during insertion into porcine heart sample.

It can be seen that when the needle is inserted slowly, the tissue experiences substantial elastic loading prior to the onset of cutting. Once the critical cutting force is met, the stored potential energy is released and the cut depth (not shown) is observed to increase suddenly. While stable cutting follows, (displacement  $> -0.002$ ), cut depth is unstable and cannot be controlled for depths less than 0.008m.

When the needle velocity is increased, although the signal noise is increased due to mechanical noise in the linear actuator, it can be seen that both the needle force and the displacement necessary to initiate cutting decrease. At this velocity, a small release in potential energy is observed as a reduction in needle force prior to stable cutting. In this case, minimum cut depth is reduced to about 0.006m.

Fig. 9 depicts peak cutting force versus needle velocity for all trials. This figure is qualitatively equivalent to Fig. 4.

Additional trials revealed that this curve results from the composite structure of the tissue, consisting of a thin outer epicardial layer and a thick underlying myocardial layer.

Needle cutting tests of the myocardial tissue reveal a flat cutting force versus velocity curve without any elastic transition to stable cutting. The force required for this stable cutting was always between .4 and .6 N. It can be seen in Fig. 9 that this is the lower bound to the reduction in cutting force with increased velocity. At velocities above  $\dot{s}_{cr} \approx 0.075$  m/s, the cutting force of the underlying myocardium is the limiting factor, and it is velocity independent. Only the outer epicardial layer exhibits a strain rate dependent cutting force.

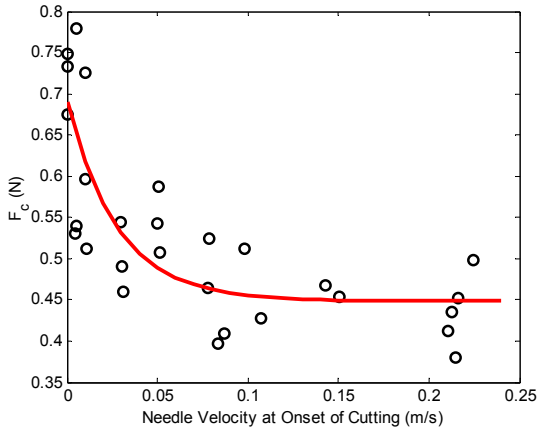


Fig. 9 Force required to initiate cutting vs. needle velocity at time of initial cutting in porcine heart sample.

#### B. Rabbit Testing

To approximate human fetal hearts, a small number of rabbit models were used in which the left ventricle diameter was approximately 1 cm. The needle target corresponds to penetration of the needle into the chamber of the ventricle. The minimum requirement for this to be achieved is that cutting ensues prior to collapse of the ventricle. In practice, however, substantial deformation of the heart is harmful and also requires needle steering.

Tests were performed approximately 10 minutes postmortem with the chest open. During these tests, the heart was still filled with fluid and supported in the chest by the surrounding tissue and organs. Fig. 10 shows needle force vs. displacement curves for representative slow and fast needle velocities. Similar to Fig. 8, cutting force and displacement decrease with increasing velocity. This decreased cutting force shows that similar to the porcine model, the rabbit myocardium also has a negatively sloped curve of cutting force vs. velocity. Since the ventricular wall is only approximately 1mm thick, as soon as cutting is initiated, the entire myocardium is penetrated, and phase II cutting is never observed. In the high speed curve of Fig. 9, the decrease in force at .014 m is where the needle enters the heart chamber. The force immediately after the peak is due to friction as the needle advances through the chamber and the subsequent rise in force is the needle loading against the back wall of the ventricle. It can be seen in Fig. 9 that penetration into the ventricle was achieved with needle

displacements of 14mm and 25 mm for slow and fast needle velocities respectively. This decreased displacement shows the results of decreasing cutting force and increasing rate dependent reaction forces by increasing needle velocity.

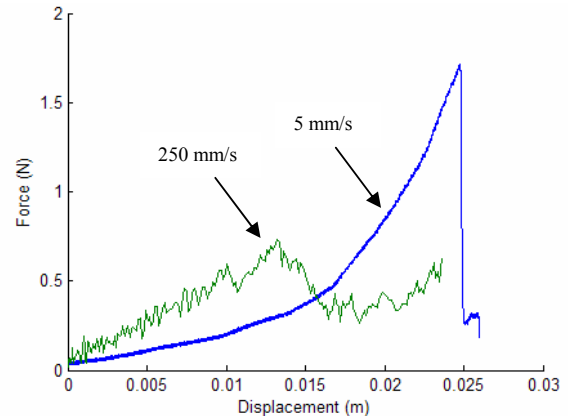


Fig. 10 Needle force vs. needle position during in-vivo rabbit heart testing.

Several closed chest tests were also performed with the rabbit models to best approximate the conditions of the human fetal procedures. During these tests, the needle was placed against the beating heart wall through a small incision in the chest under ultrasound guidance. The needle was then advanced into the left ventricle at varying insertion velocities.

Fig. 11 and Fig. 12 contrast slow and fast needle velocities in ultrasound images. In both cases, the needle displacement  $x_n$  was 17 mm. For the low-speed case of  $\dot{x}_n = 5$  mm/s shown in Fig. 11, substantial displacement and collapse of the heart has occurred without the onset of cutting. Fig. 12, which depicts the needle inside the heart, employed a needle velocity of  $\dot{x}_n = 250$  mm/s. At these speeds, needle cutting occurred reliably without noticeable deformation or displacement in the ultrasound image.



Fig. 11 Ultrasound image during 5 mm/s in-vivo insertion test showing displaced heart without penetration at end of needle stroke.

Note: needle is represented by arrow in image for clarity.



Fig. 12 Ultrasound image during 250 mm/s in-vivo insertion test showing result of high speed insertion with little heart displacement.

Note: needle is represented by arrow in image for clarity.

## V. CONCLUSIONS

It has been shown that in some important applications of needle cutting, minimizing the displacement and deformation of the tissue can be achieved by maximizing needle velocity. This equates to minimizing the cutting force and taking advantage of the rate dependent tissue reaction forces. In-vitro as well as in-vivo testing substantiates the analysis.

Current medical practice dictates slow-motion needle insertions in which trajectory corrections are made to compensate for tissue motion and deformation. High insertion speeds are avoided due to the lack of manual precision during “jabbing” motions. Automated needle insertion would be an effective technique by which extremely high needle velocities could be achieved while precisely controlling cutting depth – and simultaneously preserving the surgeon’s ability to “manually” position and aim the needle at the tissue target.

## ACKNOWLEDGMENTS

This publication was made possible by Grant Number EB003052 from NIH/NIBIB. The authors would like to thank Dr. Lisa Bergersen for her assistance with the in-vivo testing and Dr. Yoshihiro Suematsu for his assistance with the porcine heart samples.

## REFERENCES

- [1] B. Maurin, L. Barbe, B. Bayle, P. Zanne, J. Gangloff, M. DeMathelin, A. Gangi, L. Soler, and A. Forgiore “In Vivo Study of Forces During Needle Insertions” *Proceedings of the Medical Robotics, Navigation, and Visualization Scientific Workshop*, March, 2004.
- [2] A. Bzostek, R. Kumar, L. Diaz, M. Srivastava, J. Anderson, R. Taylor, “Force vs. Deformation in soft tissue puncture” *unpublished*.
- [3] T. Dang, T. Annaswamy, M. Srinivasan, “Development and Evaluation of an Epidural Injection Simulator with Force Feedback for Medical Training” *Medicine Meets Virtual Reality*, pp. 97-102, January 2001.
- [4] L. Hiemenz, J. McDonald, D. Stredney, D. Sessanna, ”A Physiologically Valid Simulator for Training Residents to Perform an Epidural Block,” *IEEE Biomedical Engineering Conf.*, pp. 170-173, 1996.
- [5] P. Yen, R. Hibberd, B. Davies, “A Telemanipulator System as an Assistant and Training Tool for Penetrating Soft Tissue” *Mechatronics*, vol. 6, no. 4, pp. 423-436, 1996.
- [6] P. Brett, A. Harrison, T. Thomas “Schemes for the Identification of Tissue Types and Boundaries at the Tool Point for Surgical Needles” *IEEE Transaction on Information Technology in Biomedicine*, Vol. 4, No. 1, March 2000.
- [7] H. Kataoka, T. Washio, K. Chinzei, K. Mizuhara, C. Simone, A. Okamura “Measurement of the Tip and Friction Force Acting on a

Needle during Penetration” *Fifth International Conference on Medical Image Computing and Computer Assisted Intervention 2001*, Vol. 2488, pp. 216-233, September, 2002

- [8] M. O’Leary, C. Simone, T. Washio, K. Yoshinaka, A. Okamura, “Robotic Needle Insertion: Effects of Friction and Needle Geometry” *IEEE International Conference on Robotics & Automation*, pp. 1774-1780, September 2003.
- [9] A. Okamura, C. Simone, M. O’Leary “Force Modeling for Needle Insertion Into Soft Tissue” *IEEE Transactions on Biomedical Engineering*, Vol. 51, No. 10, 2004, in press.
- [10] S. DiMaio, S. Salcudean “Needle Insertion Modeling and Simulation” *IEEE Transaction on Robotics and Automation Special Issue on Medical Robotics*, October 2003.
- [11] S. DiMaio, S. Salcudean, “Needle Steering and Model-Based Trajectory Planning,” *Sixth International Conference on Medical Image Computing and Computer-Assisted Intervention*, pp 33-40, November 2003.
- [12] R. Alterovitz, J. Pouliot, R. Taschereau, I. Hsu, K. Goldberg, “Simulating Needle Insertion and Radioactive Seed Implantation for Prostate Brachytherapy” *The 11<sup>th</sup> Annual Medicine Meets Virtual Reality Conference*, pp. 19-25, January, 2000.
- [13] P. Brett, T. Parker, A. Harrison, T. Thomas, and A. Carr, “Simulation of resistance forces acting on surgical needles” *Proc Instn Mech Engrs*, Vol. 211, Part H, pp. 335-347, 1997.
- [14] T. Chanthasopeephan, J. Desai, A. Lau “Study of Soft Tissue Cutting Forces and Cutting Speeds” *The 12<sup>th</sup> Annual Medicine Meets Virtual Reality Conference*, pp. 56-62, January 2004.
- [15] M. Mahvash and V. Hayward, “Haptic Rendering of Cutting: A Fracture Mechanics Approach” *Haptics-e*, Vol. 2, No. 3, November 2001.
- [16] A. Atkins and Y-W. Mai, *Elastic and Plastic Fracture: metals, polymers, ceramics, composites, biological materials*, New York: Halsted Press, 1985.